Geochemical Perspectives Letters

Magma properties at deep Earth's conditions from electronic structure of silica

S. Petitgirard[1*], C.J. Sahle[2], C. Weis[3], K. Gilmore[2], G. Spiekermann[4], J.S. Tse[5], M. Wilke[4], C. Cavallari[2], V. Cerantola[2], C. Sternemann[3]

OPEN ACCESS

doi: 10.7185/geochemlet.1902

Abstract

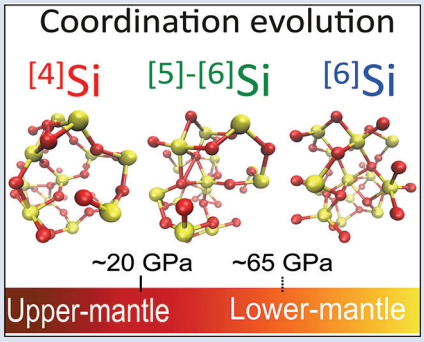

SiO_2 is the main component of silicate melts and thus controls their network structure and physical properties. The compressibility and viscosities of melts at depth are governed by their short range atomic and electronic structure. We measured the O K-edge and the Si $L_{2,3}$-edge in silica up to 110 GPa using X-ray Raman scattering spectroscopy, and found a striking match to calculated spectra based on structures from molecular dynamic simulations. Between 20 and 27 GPa, $^{[4]}$Si species are converted into a mixture of $^{[5]}$Si and $^{[6]}$Si species and between 60 and 70 GPa, $^{[6]}$Si becomes dominant at the expense of $^{[5]}$Si with no further increase up to at least 110 GPa. Coordination higher than 6 is only reached beyond 140 GPa, corroborating results from Brillouin scattering. Network modifying elements in silicate melts may shift this change in coordination to lower pressures and thus magmas could be denser than residual solids at the depth of the core-mantle boundary.

Received 8 October 2018 | Accepted 21 December 2018 | Published 6 February 2019

Letter

The entrainment or settling of silicate melts in the deep Earth is related to their physical properties, such as density and viscosity. These properties are linked to the atomic structure that controls their ascent or settling in the deep mantle. SiO_2 is the main component of silicate melts and is often used as a reference model to compare with the behaviour of other amorphous silicate compounds (Murakami and Bass, 2010) and melts at high pressure (Sanloup *et al.*, 2013) because of its network forming nature in silicate magmas. Most of the data on SiO_2 glass at high pressure have been obtained by X-ray diffraction (XRD) and show a change in the average coordination number (CN) from four- to six-fold starting at ~20 GPa and completing at pressures as low as 40 GPa (Benmore *et al.*, 2010; Sato and Funamori, 2010). Between 40 and 130 GPa, it is unclear whether the CN increases above 6 (Prescher *et al.* 2017) or plateaus around 6 (Sato and Funamori, 2010) before increasing further above 140 GPa (Wu *et al.*, 2012). Brillouin spectroscopy measurements also suggest an increase in velocities, possibly related to a CN higher than six-fold, at pressures above ~140 GPa for SiO_2, 130 GPa for $MgSiO_3$, and 110 GPa for Al-rich silicates (Murakami and Bass, 2010, 2011; Ohira *et al.*, 2016).

Many studies reported significant structural changes in silicate glasses at high pressure with potentially similar Si coordination changes in glasses and melts (Karki *et al.*, 2007; Benmore *et al.*, 2010; Sato and Funamori, 2010; Wu *et al.*, 2012; Sanloup *et al.*, 2013). Such changes seem also independent of the measurement time as illustrated by the first sharp diffraction peak position measured within hours (Sato and Funamori, 2010), minutes (Benmore *et al.*, 2010; Prescher *et al.*, 2017), or even a few seconds (Sanloup *et al.*, 2013). Similarly, density measurements of SiO_2 glasses are in very good agreement with each other, regardless of the starting glass material (Meade and Jeanloz, 1987; Petitgirard *et al.*, 2017), and are also in agreement with the quenched liquid from molecular dynamic (MD) simulations (Wu *et al.*, 2012). Still, the mechanisms associated with such high densification and compressibility (Petitgirard *et al.*, 2017) and their link to local structural changes, remains debated (Sato and Funamori, 2010; Prescher *et al.*, 2017) and requires more precise investigations on the changes in local structure with pressure.

The discrepancy in CN evolution arises because of the use of non-elemental specific probes and due to the fact that XRD and Brillouin spectroscopy measurements only give access to the bulk structure and cannot probe the electrons directly involved in the chemical bonds that reflect structural

1. Bayerisches Geoinstitut, University of Bayreuth, Bayreuth, D-95490, Germany
2. European Synchrotron Radiation Facility, 71 Avenue des Martyrs, Grenoble 38043, France
3. Fakultät Physik / DELTA, Technische Universität Dortmund, D-44221 Dortmund, Germany
4. Institut für Geowissenschaften, Universität Potsdam, Potsdam, Germany
5. Department of Physics and Engineering Physics, University of Saskatchewan, Saskatoon, Saskatchewan S7N 5E2, Canada
* Corresponding author (email: sylvain.petitgirard@erdw.ethz.ch)

rearrangements. Determining the pair distribution function (PDF) from X-ray total scattering (XRD) requires other parameters such as the density and careful background subtraction in order to obtain the average CN, and thus is not a direct method. Furthermore, natural systems with several cations (Si, Mg, Ca, Al, Fe) would be very complicated to analyse with XRD due to the overlap of cation-oxide contributions in the PDF. For instance, the CN of Si and Mg as well as the individual Si-O and Mg-O bond distances could not be solved using PDF in a recent report on $MgSiO_3$ glass (Kono *et al.*, 2018), and requires complementary analyses as well as further improvement in high pressure PDF studies.

X-ray Raman scattering (XRS) (Sternemann and Wilke, 2016 and reference therein) spectroscopy allows for measurements of X-ray absorption edges of light elements relevant for Earth compositions (Si, Mg, Al, Ca, S, O, Fe) using X-ray energies of 9.7 keV with a resolution of 0.7 eV. Only a few experiments have reported data using XRS on silica at high pressure on the O K-edge (Lin *et al.*, 2007) and on the Si L-edge (Fukui *et al.*, 2008). However, the last report does not show any evidence for changes in Si CN, because of low signal and energy resolution, and concluded that Si remains predominantly 4-fold coordinated up to 74 GPa.

Here we report XRS measurements on both Si $L_{2,3}$- and O K-edges in SiO_2 up to 110 GPa with twice the pressure range and data measured in one run, with a three-fold improvement in energy resolution at 0.7 eV. Such quality and resolution are now possible thanks to: i) the new spectrometer at the ID20 beamline at the ESRF, ii) development of diamond anvils of 500 µm thickness, allowing a five-fold gain in transmission, and iii) a new data extraction scheme. We complemented our measurements on the quenched SiO_2 melt at high pressure with first principles spectral calculations by solving the Bethe-Salpeter equation (BSE) using the OCEAN code (Gilmore *et al.*, 2015) based on trajectories from *ab initio* molecular dynamics (AIMD) simulations by Wu *et al.* (2012). (See Supplementary Information for experimental and calculation details).

We found a striking match between our experimental spectra of cold compressed glass and the calculated spectra of the quenched high pressure melt with: (i) two major discontinuities at ~20 GPa and ~60 GPa, and (ii) similar structures for the glass and the quenched melt from MD simulation. In addition, we measured the six-fold coordinated reference stishovite up to 60 GPa. It shows that Si in the glass does not reach complete 6-fold coordination at high pressure, but rather only approaches a CN of 6 at 110 GPa as corroborated by the MD simulations. At the same time, O fulfills 3-fold coordination at 40 GPa. With this unique data set we can establish the electronic and coordination changes in SiO_2 to core-mantle boundary (CMB) pressures, influencing the macroscopic properties of SiO_2.

Our experimental data show significant changes in shape for both the Si $L_{2,3}$-edge (Fig. 1a) and O K-edge (Fig. 1c) at high momentum transfer (|q|). These changes are observed for both edges at similar pressures and are well reproduced by our calculated spectra (Fig. 1b-d; spectra were shifted in energy loss to the experimental edge onsets). We report precise edge onsets as a function of pressure for both elements from our experimental data for the glass up to 110 GPa and the reference stishovite up to 60 GPa. All the data for Si low |q|, stishovite spectra and edge onset values can be found in the Supplementary Information (Figs. S-2, S-3, S-6 and Table S-1).

We did not observe changes in the spectra in the first 14-17 GPa and confirm that four-fold coordinated $^{[4]}$Si (Figs. 2, 3) remains predominant. At 17 GPa, the peak ratio of the Si $L_{2,3}$-edge spectra changes with a reduction of the second peak at 108.5 eV and a shift of the edge onset from 104.9 eV (at ambient) to 105.3 eV (at 17 GPa). Between 19 and 27 GPa we observed that the two peaks merge into a broader single peak (Fig. 1a) with a clear edge onset shift to higher energy of 106.2 eV (Fig. 2a). For the O K-edge, rapid changes between 17 and 19 GPa were also observed, with a second peak appearing at ~544.7 eV (Fig. 1c) and the edge onset shifting from 536.3 eV (ambient) to 536.7 eV (at ~19 GPa) and up to 537.4 eV at ~27 GPa

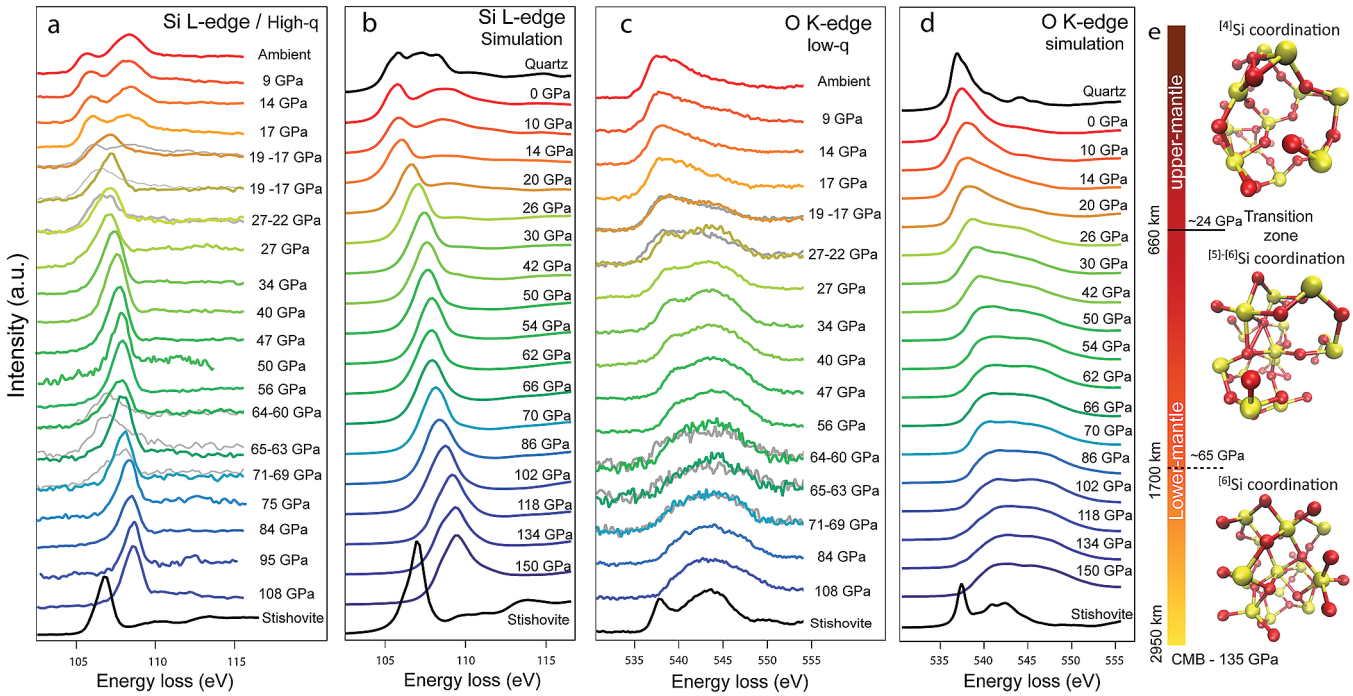

Figure 1 XRS spectra of Si $L_{2,3}$ and O K-edge up to 110 GPa from experiment and calculations. **(a,b)** Si $L_{2,3}$ spectra. **(c,d)** O K-edge spectra. Grey spectra in **a** and **c** show measurements at the starting pressure indicated on the right, the coloured spectra correspond to the final pressure. **(e)** Atomic structure of SiO_2 from MD.

(Fig. 2b). The latter illustrates an evolution of coordination also for the oxygen atoms. These changes in spectral shapes are associated with a slight drop in pressure of 2 to 5 GPa during the measurements (Figs. 1, 2). Above 27 GPa, the edge onset of both edges increases linearly with pressure: the Si L-edge reaches 107.0 eV and the O K-edge 538.6 eV at 56 GPa. Our data on stishovite compressed to 63 GPa show a linear trend of the edge onset for this canonical 6-fold reference phase, for both edges. All the Si L-edge onset values for the glass fall below that of stishovite, but tend to approach similar values around 60 GPa (Fig. 2a). For oxygen, the edge onset of the glass becomes similar to that of stishovite at around 30 GPa. This indicates that the oxygen coordination (O-Si) in the glass approaches quite rapidly a CN of 3, like that in stishovite at such pressure (Fig. 2b). This observation is consistent with a mixture of 5- and 6-fold coordinated Si at these pressures and likely pinpoints the disappearance of $^{[4]}$Si. Further, it may even indicate that Si is arranged in a mixture of edge-sharing octahedra and trigonal bipyramids, as both polyhedra require O with CN of 3. Such fine features in the electronic topology of O and Si can only be addressed using XRS, which measures the electrons directly involved in the bonding.

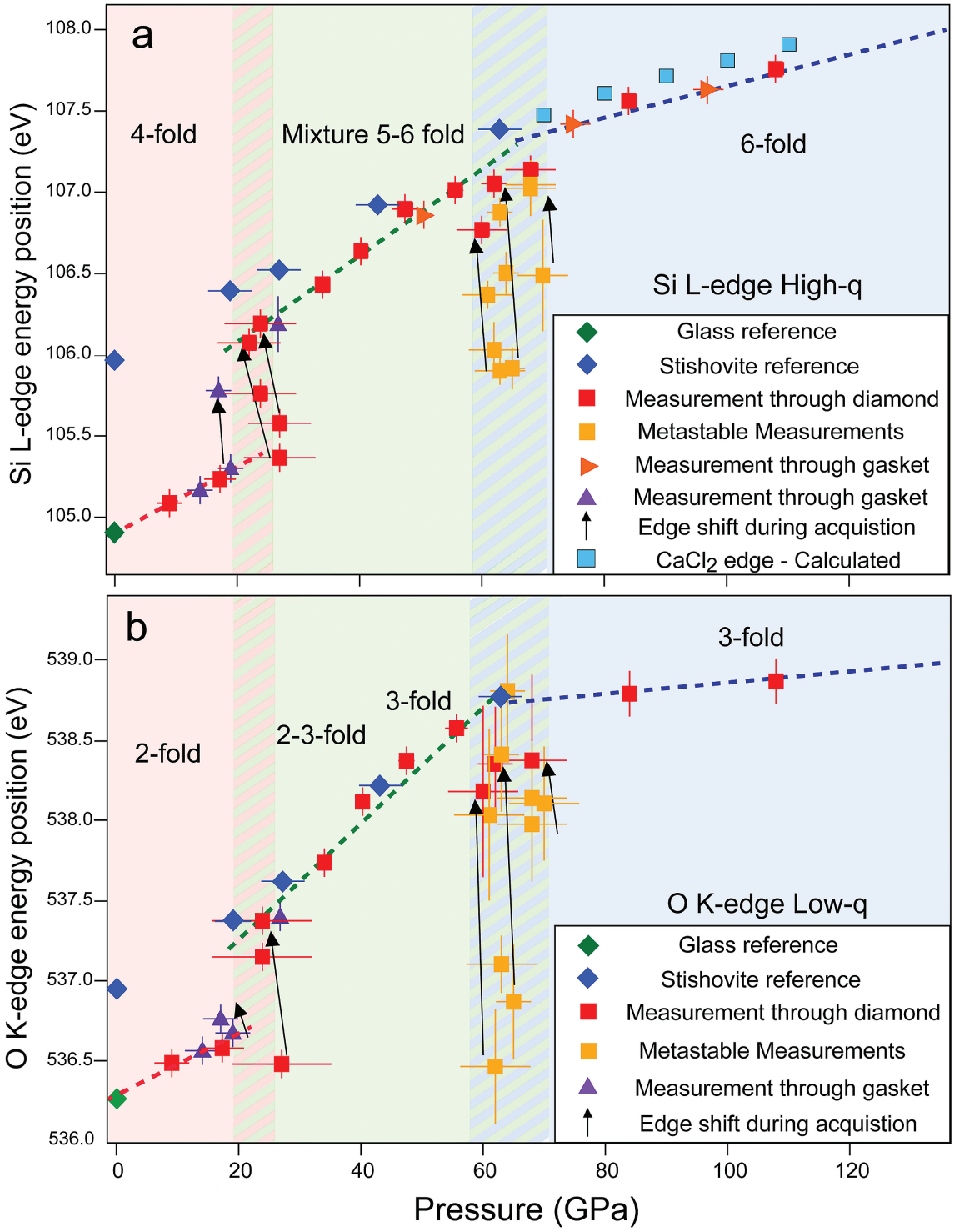

Figure 2 **(a)** Silicon $L_{2,3}$- and **(b)** Oxygen K-edge onset position *versus* pressure (GPa). Arrows show the evolution of the edge during the measurement at ~20 GPa and ~60 GPa.

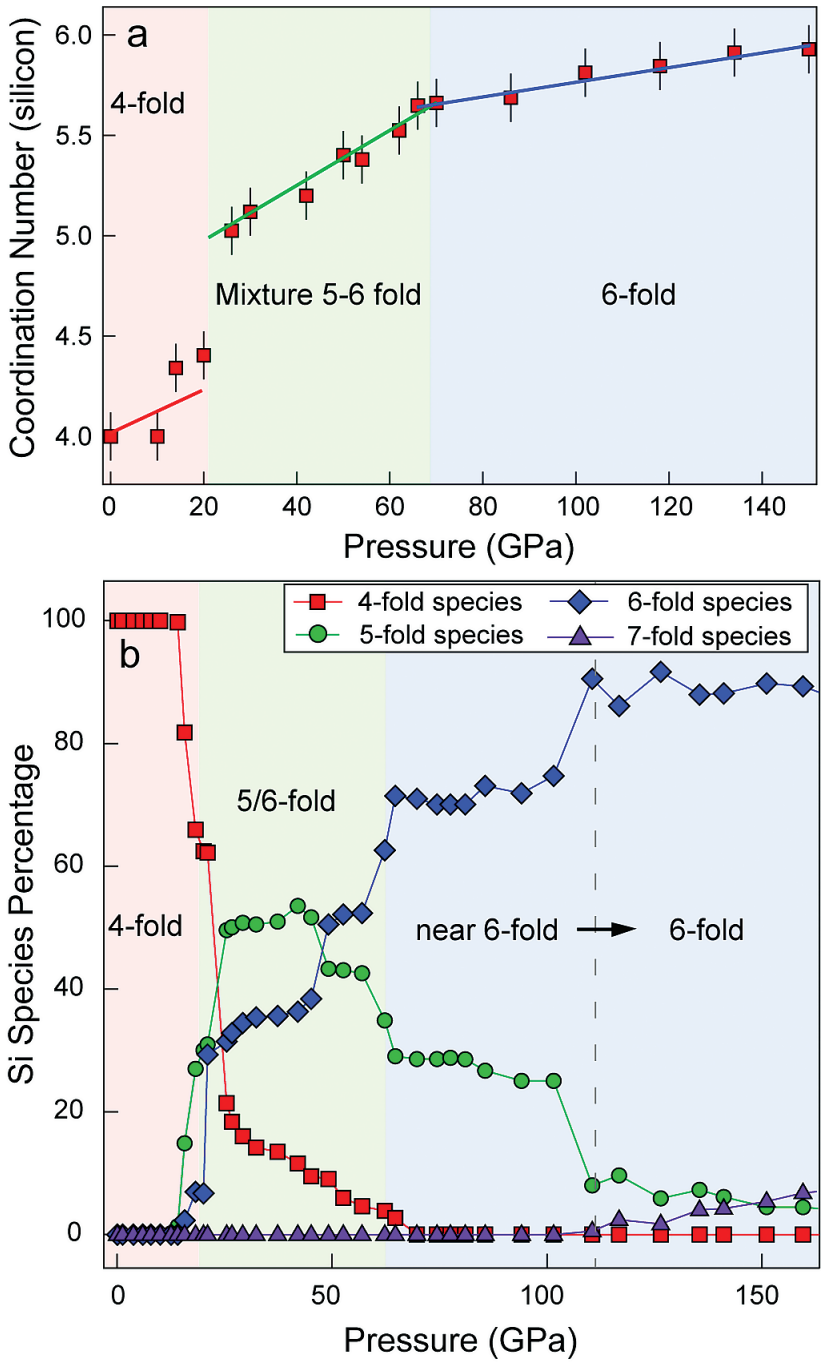

Figure 3 Coordination evolution of SiO_2 from MD. **(a)** Coordination of Si as a function of pressure. **(b)** Percentage of species $^{[4]}Si$, $^{[5]}Si$, $^{[6]}Si$ and $^{[7]}Si$.

The calculated spectra of the quenched melt from MD show similar changes, although the peak ratio changes at lower pressure (14 GPa, Fig. 2b). These changes are completed for both edges at 26 GPa, similar to the experiment. Above this transition, at 27 GPa, spectra for both edges resemble the ambient stishovite reference with a single peak for the Si $L_{2,3}$-edge and a doublet for the O K-edge (Fig. 1a-d). These spectral shapes could indicate that the 6-fold CN has been completed for a pressure as low as 30 GPa. However, our MD simulations indicate that between 20 to 27 GPa, a rapid decrease of $^{[4]}Si$ occurs, which is replaced by a mixture of an intermediate five-fold coordinated $^{[5]}Si$ species with $^{[6]}Si$ up to 60 GPa (Fig. 3b). The calculated spectra for both $^{[5]}Si$ and $^{[6]}Si$ are nearly identical with only minor differences, which explains the aspect of the Si L-edge of glass being similar to the 6-fold spectra. The lack of a $^{[5]}Si$ reference for SiO_2 combined with the similarity of $^{[5]}Si$ and $^{[6]}Si$ spectra makes it difficult to observe a distinct signal of $^{[5]}Si$ in experimental and calculated spectra (Fig. S-4).

At 60 GPa, our data show a further transition, with a broadening of the silicon peak (Fig. 1a) and an edge onset shift for both edges during the measurements (Fig. 2; detailed in Fig. S-5). Such changes are due to a re-arrangement of the glass structure. We also noticed a slight drop of pressure, which is likely related to a considerable structural change such as observed near the 20 GPa transition. Further, above 70 GPa, the Si L-edge onset in the glass still remains lower than the 6-fold $CaCl_2$ reference coordinated structure (Fig. 2). In this pressure range, between 60-70 GPa, the MD simulations indicate a clear drop in $^{[5]}Si$ species and an increase of $^{[6]}Si$

(Fig. 3b). Thus, we interpret this transition as a near completion of six-fold coordination and disappearance of $^{[5]}$Si. It is also possible that the structural re-arrangement at 60 GPa mimics the stishovite to $CaCl_2$ transition in the solid as observed for the $MgSiO_3$ system (Kono *et al.*, 2018). However, the signatures of the transition are consistent with the one at ~20 GPa which marked the disappearance of $^{[4]}$Si for a mixture of $^{[5]}$-$^{[6]}$Si. We can also observe that the shift of edge onset with pressure for both Si and O (Fig. 2a,b) follows exactly the trend given by the CN evolution as a function of pressure from MD simulations (Fig. 3a). The changes in slope for the different domains of Si species from MD (Fig. 3a,b) are in perfect agreement with our measured edge onset shift with pressure. Thus, we can interpret the breaks in the edge onset slopes as a function of pressure as a good marker for the Si coordination change.

Above 60-70 GPa, measured and calculated spectra agree very well up to 110 GPa (Figs. 1, 3). The spectral shape remained similar with a shift of both edge onsets to higher energies (Fig. 2a,b). The MD calculations show that $^{[7]}$Si-coordination only starts to appear at ~110 GPa and becomes significant at ~150 GPa (Fig. 3b), corroborating Brillouin spectroscopy measurements with an observed increase of sound velocities at such pressure in SiO_2 (Murakami and Bass, 2010). It seems unlikely that a CN > 6 is formed at pressures above 60 GPa, because there is no evidence of a further densification of SiO_2 glass compared to crystalline phases (Petitgirard *et al.*, 2017), unlike in GeO_2 for which a CN > 6 has been recorded at 60 GPa (Kono *et al.*, 2016) where the glass density may equal or even cross that of the crystal (Hong *et al.*, 2007). At 60 GPa, a change in compressibility was measured for SiO_2 (Petitgirard *et al.*, 2017) with a saturation of the density increase for higher pressure. A density crossover with solids has not been reported for SiO_2, precluding that the glass reaches a CN higher than the solid.

These results are quite different from those obtained by a recent XRD analysis (Prescher *et al.*, 2017), which suggests an average CN of 6 or higher for pressures of 40 GPa and above, but more consistent with a previous report that show a plateau of CN = 6 at around 40 GPa (Sato and Funamori, 2010). Our data show a more detailed analysis of the CN with a mixture of five- and six-fold species in this pressure range. The average CN calculated from XRD should be viewed carefully because of the large uncertainties (at least 10 %) associated with the method. Our XRS measurements, confronted to the canonical 6-fold reference systems using the same technique, give a direct and precise coordination for Si using the edge onset shift. XRS measurements also yield information on the oxygen coordination, evolving from $^{[2]}$O to $^{[3]}$O with a completion at lower pressure than for Si. Thus, XRS brings important evidence that the electronic shell around the two atoms can be compressed and re-arranged in a different way than the simple hard sphere model would explain (Du and Tse, 2017), which is often used to model the oxygen packing fraction. The same compression mechanism takes place in GeO_2 glass as measured with X-ray emission spectroscopy (Spiekermann *et al.*, 2019). A CN above 6 for Si may only form for pressures above 140 GPa with a significant increase of $^{[7]}$Si species as suggested by the MD results (Fig. 3b). The increase in sound velocity in SiO_2 at 140 GPa measured by Brillouin spectroscopy (Murakami and Bass, 2010) could then be due to a densification of the glass linked to an evolution of the CN of Si above 6 (Wu *et al.*, 2012).

In summary, we find a striking match between the spectra obtained from experimental data and the ones calculated from the quenched melt (Figs. 1, S-2, S-4). We observe two structural changes at ~20 GPa and ~60 GPa related to changes of the electronic environment of Si and O. This may also occur in silicate melts (Sanloup *et al.*, 2013), with large influences on the chemical and physical properties of melts at such pressures, such as change in melt viscosity (Meade and Jeanloz, 1988) or partitioning of elements (Sanloup *et al.*, 2013). In the context of a magma ocean, it may affect the chemical segregation, thermal evolution of the CMB, and mobility of melts during magma crystallisation. The transition at 60-70 GPa is quite marked in the glass and corresponds to the near-disappearance of the $^{[5]}$Si in favour of the $^{[6]}$Si species in the quenched melt (Fig. 2b). This provides a good explanation for the change of compressibility at such pressures in the density data (Petitgirard *et al.*, 2017), but also for the variation of strength of the glass (Meade and Jeanloz, 1988). Our MD results indicate that silica does not exceed six-fold coordination at pressures of the deep mantle (Fig. 3b). Depolymerised melt compositions, containing network modifying cations (*e.g.*, Mg, Ca, Al) have shown stronger densification at lower pressures, closer to the CMB as illustrated by Brillouin measurements on $MgSiO_3$ and Al-rich SiO_2 (Ohira *et al.*, 2016) glasses. The depolymerised nature of such compositions would facilitate the increase of CN > 6 for Si at pressures of the lower mantle producing negatively buoyant silicate at the CMB during the early Earth's formation or today in the modern mantle.

Acknowledgements

We acknowledge the ESRF for provision of beamtime under the proposal ES-431. We acknowledge N. Dubrovinskaia for providing us the stishovite standard material. We wish to thank Dr. Yunfeng Liang for providing the *ab initio* MD trajectories used in this study. We acknowledge the support of ID20 beamline staff, M. Moretti Sala and C. Henriquet. SP is financed by a DFG grant (PE 2334/1-1). The Scios Focus Ion Beam at BGI was financed by a DFG grant No. INST 91/315-1 FUGG. CS and CW would like to thank M. Tolan for discussion and general support of these activities and acknowledge funding by the BMBF (05K13PE2 and 05K16PE1).

Editor: Simon Redfern

Additional Information

Supplementary Information accompanies this letter at http://www.geochemicalperspectivesletters.org/article1902.

Cite this letter as: Petitgirard, S., Sahle, C.J., Weis, K., Gilmore, K, Spiekermann, G., Tse, J.S., Wilke, M., Cavallari, C., Cerantola, V., Sternemann, C. (2019) Magma properties at deep Earth's conditions from electronic structure of silica. *Geochem. Persp. Let.* 9, 32–37.

References

Benmore, C.J., Soignard, E., Amin, S.A., Guthrie, M., Shastri, S.D., Lee, P.L., Jarger, J.L. (2010) Structural and Topological Changes in Silica Glass at Pressure. *Physical Review B* 81, 054105.

Du, X.P., Tse, J.S. (2017) Oxygen Packing Fraction and the Structure of Silicon and Germanium Oxide Glasses. *Journal of Physical Chemistry B* 121, 10726–10732.

Fukui, H., Kanzaki, M., Hiraoka, N., Qai, Y.C. (2008) Coordination Environment of Silicon in Silica Glass up to 74 GPa: An X-Ray Raman Scattering Study at the Silicon L Edge. *Physical Review B* 78, 012203.

Gilmore, K., Vinson, J., Shirley, E.L., Prendergast, D., Pemmaraju, C.D., Kas, J.J., Vila, F.D., Rehr, J.J. (2015) Efficient Implementation of Core-Excitation Bethe-Salpeter Equation Calculations. *Computer Physics Communications* 197, 109.

Hong, X., Shen, G., Prakapenka, V.B., Rivers, M.L., Sutton, S.R. (2007) Density Measurements of Noncrystalline Materials at High Pressure with Diamond Anvil Cell. *Review of Scientific Instruments* 78, 103905.

Karki, B.B., Bhattarai, D., Stixrude, L. (2007) First-Principles Simulations of Liquid Silica: Structural and Dynamical Behavior at High Pressure. *Physical Review B* 76, 104205.

Kono, Y., Kenney-Benson, C., Ikuta, D., Shibazaki, Y., Wang, Y., Shen, G. (2016) Ultrahigh-Pressure Polyamorphism in GeO2 Glass with Coordination Number > 6. *Proceedings of the National Academy of Sciences of the United States of America* 113, 3436–3441.

Kono, Y., Shibazaki, Y., Kenney-Benson, C., Wang, Y., Shen, G. (2018) Pressure-Induced Structural Change in MgSiO3 Glass at Pressures near the Earth's Core–mantle Boundary. *Proceedings of the National Academy of Sciences of the United States of America* 115, 1742–1747.

Lin, J.-F., Fukui, H., Prendergast, D., Okuchi, T., Cai, Y.Q., Hiraoka, N., Yoo, C.-S., Trave, A., Eng, P., Hu, M.Y., Chow, P. (2007) Electronic Bonding Transition in Compressed SiO2 Glass. *Physical Review B* 75, 012201.

Meade, C., Jeanloz, R. (1987) Frequency-Dependent Equation of State of Fused Silica to 10 GPa. *Physical Review B* 35, 236–244.

Meade, C., Jeanloz, R. (1988) Effect of Coordination Change on the Strength of Amorphous SiO2. *Science* 241, 1072–1074.

Murakami, M., Bass, J.D. (2010) Spectroscopic Evidence for Ultrahigh-Pressure Polymorphism in SiO2 Glass. *Physical Review Letters* 104, 025504.

Murakami, M., Bass, J.D. (2011) Evidence of denser MgSiO3 glass above 133 gigapascal (GPa) and implications for remnants of ultradense silicate melt from a deep magma ocean. *Proceedings of the National Academy of Sciences* 108, 17286.

Ohira, I., Murakami, M., Kohara, S., Ohara, K., Ohtani, E. (2016) Ultrahigh-Pressure Acoustic Wave Velocities of SiO2-Al2O3 Glasses up to 200 GPa. *Progress in Earth and Planetary Science* 3, 18.

Petitgirard, S., Malfait, W.J., Journaux, B., Collings, I.E., Jennings, E.S., Blanchard, I., Kantor, I., Kurnusov, A., Cotte, M., Dane, T., Burghammer, M., Rubie, D.C. (2017) SiO2 Glass Density to Lower-Mantle Pressures. *Physical Review Letters* 119, 215701.

Prescher, C., Prakapenka, V.B., Stefanski, J., Jahn, S., Skinner, L.B., Wang, Y. (2017) Beyond Sixfold Coordinated Si in SiO2 Glass at Ultrahigh Pressures. *Proceedings of the National Academy of Sciences* 114, 10041–10046.

Sanloup, C., Drewitt, J.W.E., Konopkova, Z., Dalladay-Simpson, P., Morton, D.M., Rai, N., van Westrenen, W., Morgenroth, W. (2013) Structural Change in Molten Basalt at Deep Mantle Conditions. *Nature* 503, 104–107.

Sato, T., Funamori, N. (2010) High-Pressure Structural Transformation of SiO2 Glass up to 100 GPa. *Physical Review B* 82, 209604.

Spiekermann, G., Harder, M., Gilmore, K., Zalden, P., Sahle, C.J., Petitgirard, S., Wilke, M., Biedermann, N., Weis, C., Morgenroth, W., Tse, J.S., Kulik, E., Nishiyama, N., Yavaş, H., Sternemann, C. (2019) Persistent Octahedral Coordination in Amorphous GeO2 Up to 100 GPa by Kβ'' X-Ray Emission Spectroscopy. *Physical Review X* 9, 011025.

Sternemann, C., Wilke, M. (2016) Spectroscopy of Low and Intermediate Z Elements at Extreme Conditions: In Situ Studies of Earth Materials at Pressure and Temperature via x-Ray Raman Scattering. *High Pressure Research* 36, 275–292.

Wu, M., Liang, Y., Jiang, J.-Z., Tse, J.S. (2012) Structure and Properties of Dense Silica Glass. *Scientific Reports* 2, 398.

Geochemical Perspectives Letters

Magma properties at Earth's lower mantle conditions inferred from electronic structure and coordination in silica

S. Petitgirard, C. Sahle, C. Weiss, K. Gilmore, G. Spiekermann, J.S. Tse, M. Wilke, C. Cavallari, V. Cerantola, C. Sternemann

Supplementary Information

The Supplementary Information includes:

- Experimental Details
- BSE Spectral Calculations
- Data Analysis Details
- Figures S-1 to S-6
- Table S-1
- Supplementary Information References

Experimental Details

X-ray Raman Scattering (XRS) measurements were performed on the ID20 beamline of the ESRF (Grenoble, France) (Huotari *et al*., 2017). The incident energy was set at 9.7 keV through a first high heat-load liquid-nitrogen cooled Si(111) pre-monochromator and a final incident bandwidth of approximately 0.4 eV was obtained using a Si(311) channel-cut post-monochromator. The beam was focused down to ~10×20μm^2 (V x H) through a pair of Kirkpatrick-Baez mirrors. Three out of six spectrometers were used to collect the scattering signal allowing to probe the sample at different transfer momenta $|q|$ up to a maximum of 10Å^{-1}. Each spectrometer contains twelve Si(660) spherically curved crystal analysers that act as focusing monochromator enabling a sub-eV (0.7 eV) final resolution when working at 9.7 keV. The sample was a SiO_2 suprasil glass, the same as for the density measurements (Petitgirard *et al., 2017)*, ground into a fine powder. We used BX90 cells from BGI and PanoDAC or new MBX110 from the ESRF sample environment pool. We performed three measurements through Be gaskets, with cBN inserts, in the PanoDAC following the procedure describe in Sahle *et al*. (2016) using standard conical diamonds with 500 μm culet size and three other measurements up to 100 GPa using 150 μm culet size using the MBX110 DAC from the ESRF pool. For most of the runs we used miniature diamond anvils of about 480 μm thickness (Petitgirard *et al*., 2016), three times thinner than the standard design in order to reduce the absorption of the incoming and scattered X-ray beams (Fig. S-1), with culets of 200 μm up to 66 GPa and 120 μm culet for the highest pressures. The amount of sample was further increased by milling two recesses of 20 μm in the culets of both anvils using a focused ion beam (FIB) at BGI, enabling an increase of sample volume by a factor of three at high pressure. The sample was loaded

into the sample chamber drilled in a 250 μm rhenium gasket pre-indented down to 40 μm thickness with a 100 micron hole and 20 μm thickness and a 60 micron hole for 200 μm culets and 120 μm culets respectively.

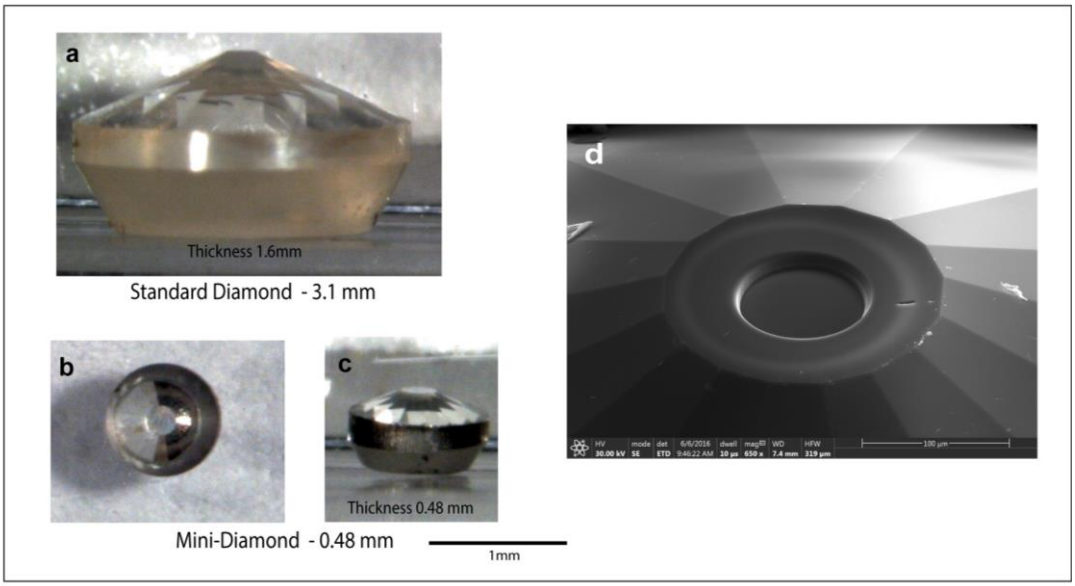

Figure S-1 Miniature diamonds for XRS experiments. **(b-c)** Mini-diamonds dimensions compared to standard diamond anvil **(a). (d)** Milling of a recess using the FIB at BGI Bayreuth.

BSE Spectral Calculations

All spectral calculations were performed on configurations sampled from the previously reported *ab initio* molecular dynamics (MD) simulations of quenched molten quartz (Wu *et al*., 2012) at multiple pressures between ambient and 150 GPa. For all the MD simulations and spectral calculations, the computational cells consisted of 24 structural units (72 atoms). At each pressure, the spectral calculations were based on 10 independent MD configurations and the momentum-dependent Si $L_{2,3}$ and O K-edge XRS spectra were computed as the sum of the excitation spectra of all the Si and O atoms in the structure. For each pressure presented in Figure 1 and Figure S-2, we extracted 10 snapshots at equally spaced time intervals of few ps and evaluated both the Si $L_{2,3}$- and O K-edge for each of the 24 Si and 48 O atoms for a total of 240 individual Si $L_{2,3}$- and 480 O K-edge spectra at each pressure point. The coordination number (CN) was estimated subject to distance cut-off criteria, *i.e.* we used the first minimum in the Si-O radial distribution function as a cut-off and used the number of oxygen atoms around a silicon atom within a sphere with this cut-off radius as the CN.

Calculations of the XRS spectra using the BSE (Bethe-Salpeter Equation) method were performed with the OCEAN code (Obtaining Core level Excitations using *Ab initio* methods and the NIST BSE solver) (Vinson *et al*., 2011). Ground state electron densities and wave functions were generated at the density functional theory (DFT) level using Quantum ESPRESSO (Giannozzi *et al*., 2009). Quantum-ESPRESSO is a community project for high-quality quantum-simulation software, based on density-functional theory, and coordinated by Paolo Giannozzi. See http://www.quantum-espresso.org and http://www.pwscf.org]. Due to the use of pseudopotentials, projector augmented wave (PAW) (Kresse and Joubert, 1998) reconstructed all electron wave functions were generated for the calculation of core to valence transition matrix elements. The dielectric screening was evaluated using a real space implementation of the random phase approximation within a short range, atom centered sphere. Outside this sphere the Levine Louie model dielectric function was used. Results are converged with respect to the change-over radius (Levine and Louie 1982).

Final electron-hole scattering states are obtained by solving the BSE. DFT calculations were performed within the local density approximation (LDA) to the exchange-correlation functional, and using norm conserving pseudopotentials taken from the ABINIT repository. We used FHI formatted pseudopotential from the http://www.abinit.org distribution. A planewave energy cutoff of 70 Ry was used for these calculations. The ground state electron density was calculated using ⊙-point sampling. The wave functions for the screening and BSE calculation were generated from a non-self-consistent-field calculation using a 2x2x2 *k*-point mesh.

Data Analysis Details

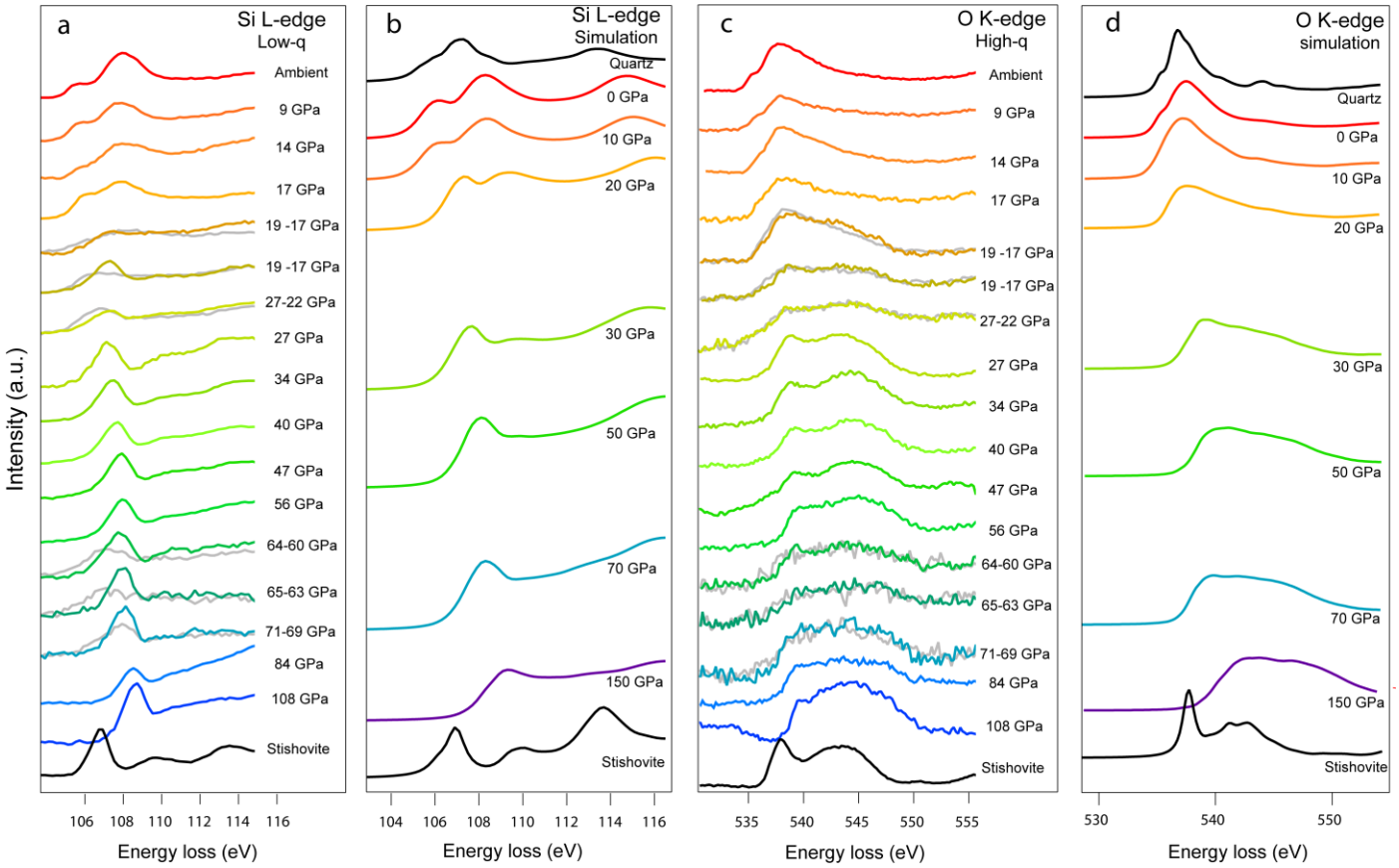

Figure S-2 XRS spectra of the Si $L_{2,3}$ at low-|q| scattering angle **(a)** and O K-edge at high-|q| scattering geometry **(b)** up 110 GPa compared to calculated spectra form MD structures for similar scattering geometry. **(a)** Si $L_{2,3}$ low-|q| measurements compared to calculated spectra in **b**. **(c)** O K-edge measurements at high-|q| compared to calculated spectra in **(d).** Grey spectra in **a** and **c** correspond to the first measurements at the highest pressure indicated on the right, the coloured spectra correspond to the final pressure. More detailed about spectra at pressure around 60 GPa can be found in Figure 4.

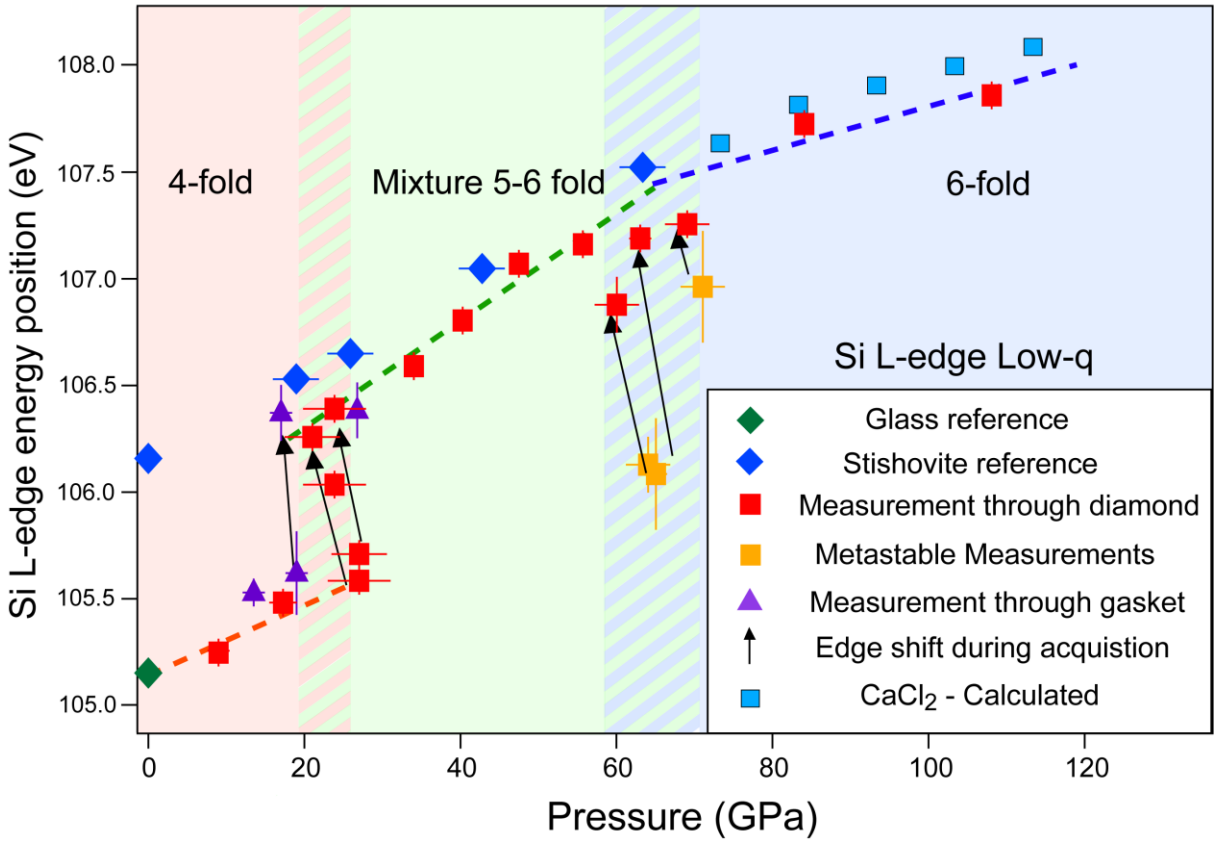

Figure S-3 Silicon edge onset as a function of pressure at low-|q| scattering geometry. As for other scattering geometry at high-|q| but also for the O K-edge, two metastable regions can be observed at ~20 GPa and ~60 GPa corresponding to coordination changes from $^{[4]}$Si to $^{[5/6]}$Si and $^{[5/6]}$Si to $^{[6]}$Si respectively.

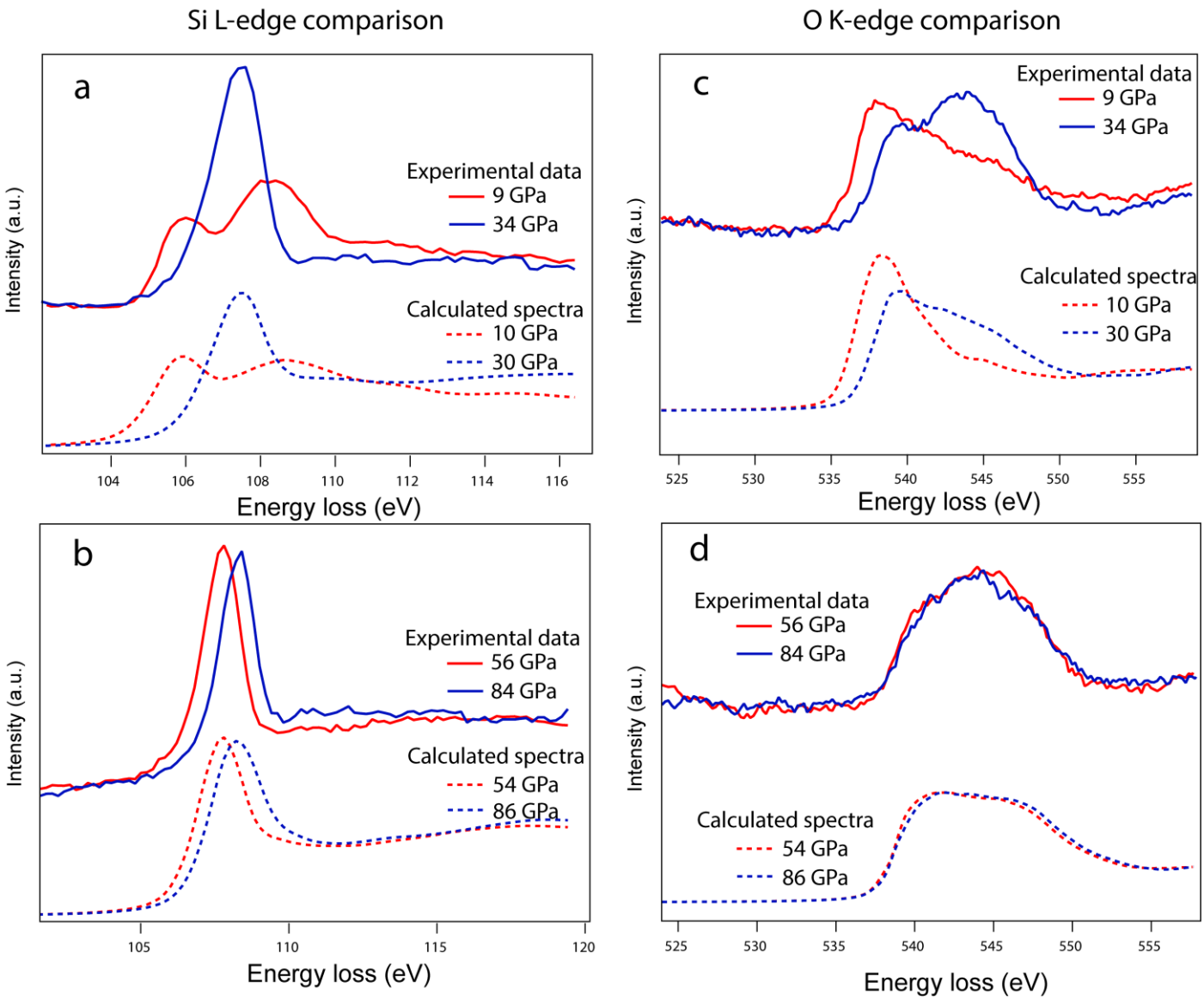

Figure S-4 Comparison between experimental data and calculated spectra from MD structures for the Si L-edge and O K-edge for pressures below and above the main coordination changes at ~20 GPa and ~60 GPa respectively.

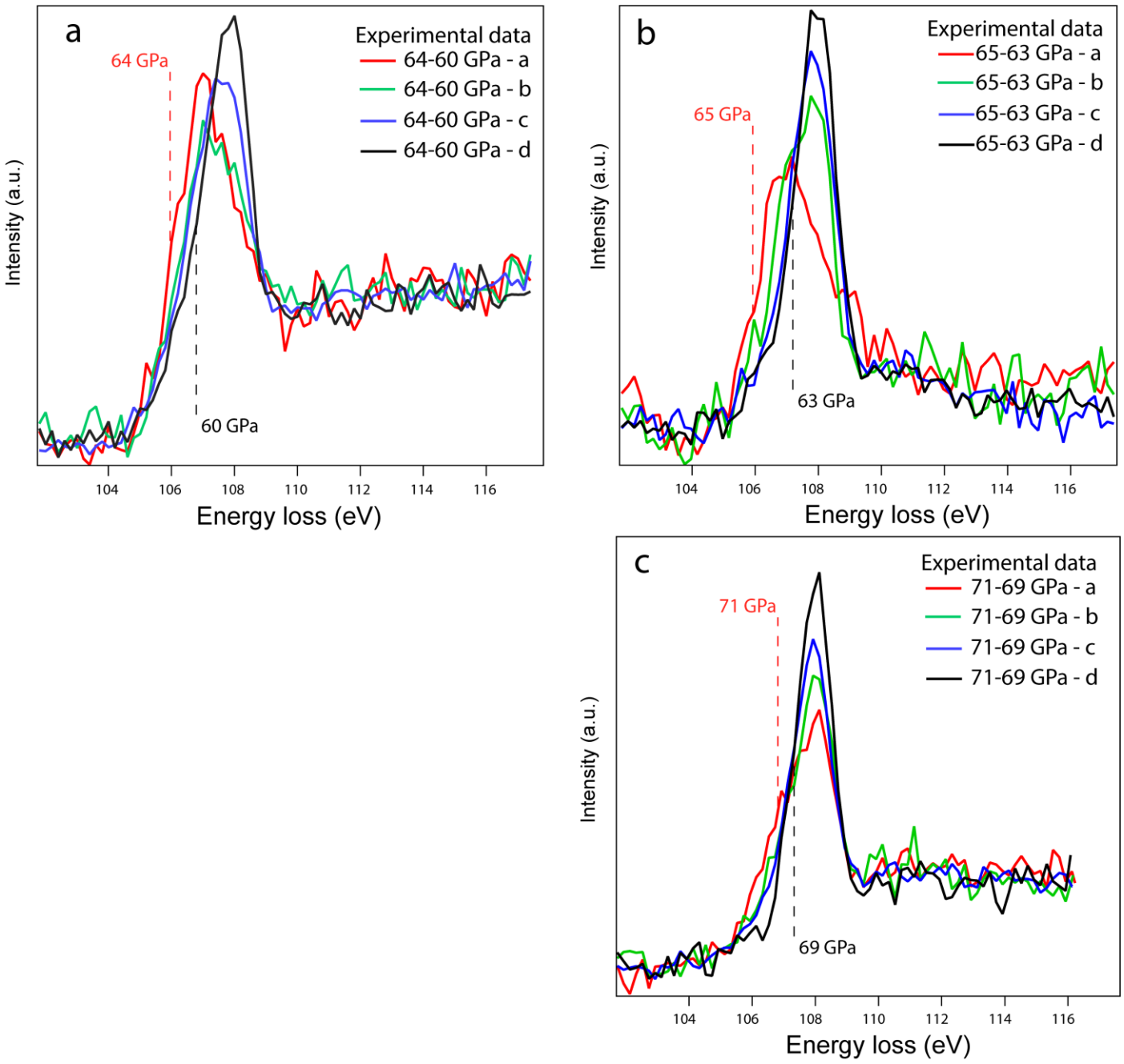

Figure S-5 Si L-edge onset detailed analysis in the metastable region between 60 to 70 GPa for three different pressures and loadings. The four energy scans of the Si L-edge are decomposed and plotted together **(a, b, c).** The pressure of the first spectra in red was measured before and the last pressure in black after the XRS measurement. In **a**, **b** and **c**, the edge onset shifts to higher energy with time while the pressure decreases. The final edge measurements are very close to the value found at lower and higher pressure emphasizing a kinetic effect in the glass for the transition from $^{[5]-[6]}$Si to $^{[6]}$Si. We did not observe such process for other pressure where the edge onset is stable over time as well as the pressure and matches perfectly the calculated spectra (Fig. 3)

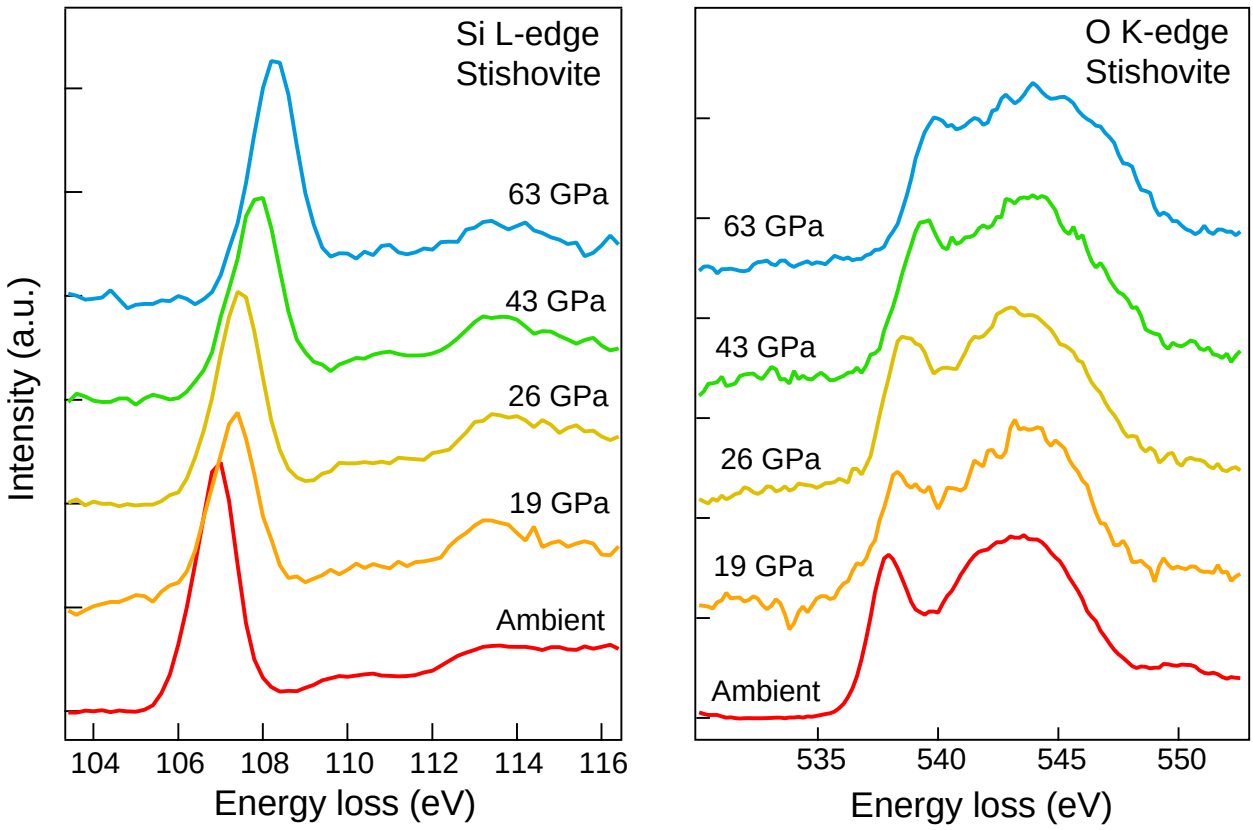

Figure S-6 XRS measurements of the Si L-edge and O K-edge of stishovite reference material under high pressure up to 63 GPa

Table S-1 Data for the edge onset measurements for both the Si L-edge and O K-edge as a function of pressure as well as reference material values for stishovite and glass. In the table, all the data collected in different geometry (through Be and through the diamonds) are reported. The bold italic numbers correspond to edge onset and pressure values of the two transitions where the spectra are changing during the measurement (around 20 GPa and 60 GPa). All other points were stable over time.

Geometry	Pressure	Si Edge Onset	Geometry	Pressure	O Edge Onset
Through Be	14.00	105.17	*Through Be*	14.00	536.56
	19.00	***105.31***		***19.00***	***536.67***
	17.00	***105.79***		***17.00***	***536.75***
	26.75	106.20		26.75	537.39
Through Diamond	9.00	105.09	*Through Diamond*	9.00	536.48
	17.25	105.24		17.25	536.57
	27.00	***105.37***		***27.00***	***536.47***
	23.85	***105.77***		***23.85***	***537.14***
	23.85	***106.20***		***23.85***	***537.37***
	27.00	***105.59***		***34.00***	***537.73***
	22.00	106.08		40.25	538.12
	34.00	106.44		47.45	538.37
	40.25	106.64		55.65	538.58
	47.45	106.90		62.00	538.18
	55.65	107.02		64.00	538.35
	62.00	106.77		69.00	538.37
	64.00	107.06		84.00	538.79
	69.00	107.14		108.00	538.87
	84.00	107.57			
	108.00	107.76			
Metastable region	***63.00***	***105.91***	*Metastable region*	***63.00***	***537.10***
	62.00	***106.04***		***62.00***	***536.46***
	61.00	***106.38***		***61.00***	***538.03***
	65.00	***105.92***		***65.00***	***536.86***
	64.00	***106.51***		***64.00***	***538.81***
	63.00	***106.88***		***63.00***	***538.41***
	70.00	***106.49***		***70.00***	***538.10***
	68.00	***107.05***		***68.00***	***537.97***
	68.00	***107.03***		***68.00***	***538.14***
Reference			**Reference**		
Stishovite	0.00	105.99	*Stishovite*	0.00	536.94
Glass	0.00	104.91	*Glass*	0.00	536.29
Stishovite	0.00	105.99	*Stishovite*	0.00	536.94
	19.00	106.41		19.00	537.38
	26.00	106.52		26.00	537.62
	43.00	106.90		43.00	538.22
	63.00	107.35		63.00	538.77

Supplementary Information References

Giannozzi, P. *et al.* (2009) QUANTUM ESPRESSO: a modular and opensource software project for quantum simulations of materials. *Journal of Physics Condensed Matter* 21, 395502.

Kresse, G., Joubert, D. (1998) From ultra-soft pseudopotentials to the projector augmented-wave method. *Physical Review B* 59, 1758.

Levine, Z.H., Louie, S.G. (1982) New model dielectric function and exchange correlation potential for semiconductors and insulators. *Physical Review B* 25, 6310.

Huotari, S. *et al.* (2017) A large-solid-angle X-ray Raman scattering spectrometer at ID20 of the European Synchrotron Radiation Facility. *Journal of Synchrotron Radiation 24*, 521–530.

Petitgirard, S. *et al.* (2016) Miniature Diamond Anvils for X-Ray Raman Scattering Spectroscopy Experiments at High Pressure. *Journal of Synchrotron Radiation* 24, 276–282

Petitgirard, S. *et al.* (2017) SiO2 Glass Density to Lower-Mantle Pressures. *Physical Review Letters* 119, 215701.

Sahle, C.J. *et al.* (2016) Direct tomography imaging for inelastic x-ray scattering experiments at high pressure. *Journal of Synchrotron Radiation* 24, 269–275.

Wu, M., Liang, Y., Jiang, J.-Z., Tse, J.S. (2012) Structure and Properties of Dense Silica Glass. *Scientific Reports* 2, 398.

Vinson, J., Rehr, J.J., Kas, J.J., Shirley, E.L. (2011) Bethe-Salpeter equation calculations of core excitation spectra. *Physical Review B* 83, 115106.